Chapter 12
Simultaneous Measurement of Force and Conductance Across Single Molecule Junctions

Sriharsha V. Aradhya, Michael Frei, Mark S. Hybertsen, and Latha Venkataraman

Abstract Measurement of electronics and mechanics of single molecules provides a fundamental understanding of conductance as well as bonding at the atomic scale. To study the mechanics at these length scales, we have built a conducting atomic force microscope (AFM) optimized for high displacement and force resolution. Here, we simultaneously measure conductance and force across single Au-molecule-Au junctions in order to obtain complementary information about the electronics and structure in these systems. First we show that single-atom Au contacts, which have a conductance of G_0 ($2e^2/h$), have a rupture force of about 1.4 nN, in excellent agreement with previous theoretical and experimental studies. For a series of amine and pyridine linked molecules which are bound to Au electrodes through an Au-N donor-acceptor bond, we observe that the rupture force depends on the backbone chemistry and can range from 0.5 to 0.8 nN. We also study junctions formed with molecules that bind through P-Au and S-Au interactions. We find that both the conductance signatures and junction evolution of covalent S-Au bond (thiolate) and a donor-acceptor S-Au bond (thiol) are dramatically different. Finally, we perform density functional theory based adiabatic molecular junction elongation and rupture calculations which give us an insight into the underlying mechanisms in these experiments.

12.1 Introduction

Understanding the physical properties of single molecule junctions is of fundamental importance to nanoscale electronics [1–7]. While the electrical and thermal properties of a variety of organic molecules bound to metal electrodes have been probed [6–14], measurements of rupture forces of single metal-molecule-metal junctions are new [15–19]. Mechanical information at these length scales can help address a multitude of untested predictions regarding the interplay between structure, mechanics and electronics of these junctions. In particular, probing the relation between mechanical and electronic properties of single molecule circuits provides a deeper understanding of the structure-conductance relation in these systems. The force signature for particular bond rupture events occurring during junction formation and evolution are probed in these measurements, similar to the more established conductance signatures for a variety of known molecular backbones and linker group combinations. However, conductance data alone is often insufficient to fully explain the complex, atomic processes that control the evolution of the junction structure, in particular under stress. In this respect, force measurements can potentially be used to determine bond rupture forces, junction stiffness, and their relation to the loading rate, that has been demonstrated for biomolecular systems [20, 21].

Here, we use a modified atomic force microscope (AFM) to form single molecule junctions between an Au substrate and an Au-coated cantilever (Fig. 12.1). The simultaneously measured conductance and force between the AFM tip and substrate are analyzed to determine bond rupture forces [17, 18]. We analyze force data to obtain bond rupture forces from a large, statistically significant set of individual measurements. We first show that the force required to break an Au-Au bond is

S.V. Aradhya • M. Frei • L. Venkataraman (✉)
Department of Applied Physics and Applied Mathematics, Columbia University, New York, NY 10027, USA
e-mail: SVA2107@columbia.edu; LV2117@columbia.edu

M.S. Hybertsen
Center for Functional Nanomaterials, Brookhaven National Laboratory, Upton, NY 11973, USA

G.A. Shaw et al. (eds.), *MEMS and Nanotechnology, Volume 6: Proceedings of the 2012 Annual Conference on Experimental and Applied Mechanics*, Conference Proceedings of the Society for Experimental Mechanics Series 42,
DOI 10.1007/978-1-4614-4436-7_12,

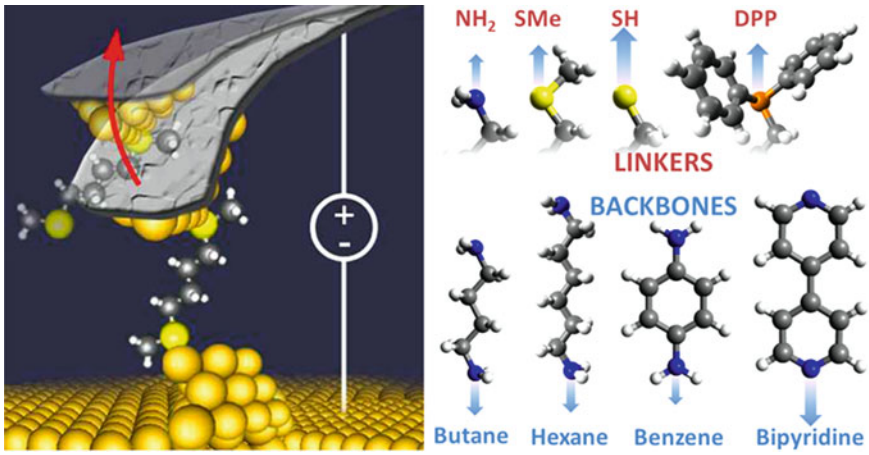

Fig. 12.1 Illustration of stretching and breaking of a single molecule junction between the AFM cantilever and the substrate. Chemical structure of the linker groups and molecular backbones measured in this study are shown along with *arrows* of size proportional to their respective measured rupture forces

1.4 nN, based on over 31,000 individual measurements and in good agreement with previous published results [22–24]. We then show that for single molecule junctions, the N-Au bond-rupture force depends on the molecular backbone, and varies from 0.8 nN for 4,4′ bipyridine to 0.5 nN in 1,4 diaminobenzene [17]. We then compare the conductance and rupture forces of single molecule junctions formed by alkane backbones terminated with four different linker groups: amine, methylsulfide, diphenylphosphine and thiol [18]. For the first three, which bind to Au through a donor-acceptor bond, we see clear conductance signatures, with junctions rupturing under 0.6–0.8 nN stress. In contrast, junctions with thiol linkers undergo multiple plastic deformation events during elongation, indicative of structural rearrangements. However, we find that these events have an average rupture force that is smaller than the 1.4 nN observed for the rupture force of a single Au atom contact. These results show that the rupture of an Au-S covalently bonded junction, which would most likely occur at an Au-Au bond, does not require a force of 1.4 nN contrary to what is commonly assumed. Finally, we perform density functional theory (DFT) calculations for adiabatic junction elongation trajectories. Chemical trends in the maximum sustained force determined from these calculations agree well with the experimental results for rupture forces.

12.2 Experimental Methods

A schematic representation of the AFM setup is shown in Fig. 12.2a. The conductive AFM consists of a modified AFM head (Veeco Multimode), external adder and filter circuits (SRS), as well as a homebuilt cantilever holder. A constant bias is applied between an Au coated cantilever (TAP300, BudgetSensors) and an Au substrate placed on top of a single-axis piezoelectric positioner with a built-in position sensor (Mad City Labs). The resulting current is converted to a voltage with a current amplifier (Keithley 428). Data collection and control of the piezoelectric positioner are done by means of a data acquisition board (National Instruments, PXI-4461) driven by a customized program using Igor software (Wavemetrics Inc.). The AFM cantilever coated with a 5 nm Chromium adhesion layer and 100 nm of Au (99.999% purity, Alfa Aesar) served as one electrode. An Au substrate (mica with 100 nm Au layer, 99.999% purity, Alfa Aesar) served as the second electrode. The cantilever and substrate were UV/ozone cleaned prior to use. Force was determined by measuring the deflections of a laser spot focused on the back of the cantilever, collected on the detector. The detector signal was calibrated to yield the force data, using the thermal power spectrum method [23, 25]. For the simultaneous conductance and force trace measurements, the substrate approached the cantilever tip until a set conductance larger than 5 G_0 was measured to ensure that the Au-molecule-Au junction from the previous measurement was completely destroyed. The sample was withdrawn at a rate of 18 nm/s and the current and force versus position data was recorded at a sampling frequency of 100 kHz. All position determinations were based on measurements with the built-in position sensor within our custom piezoelectric positioner. This position sensor was calibrated both by the manufacturer and by us using laser interference measurements. We found the absolute values of the measured displacements to be accurate to within 5%.

We simultaneously measure the conductance and force of molecular junctions by repeatedly forming and rupturing Au point contacts between the tip and substrate of the AFM (Fig. 12.2a). Simultaneous measurements of cantilever deflection relate to the force applied across the junction. The AFM is operated in ambient conditions at room temperature. Conductance is measured by applying a constant bias of 25 mV between the tip and substrate, and measuring the resulting current. For each measurement, an Au point-contact is first formed between the substrate and cantilever. It is then pulled apart and

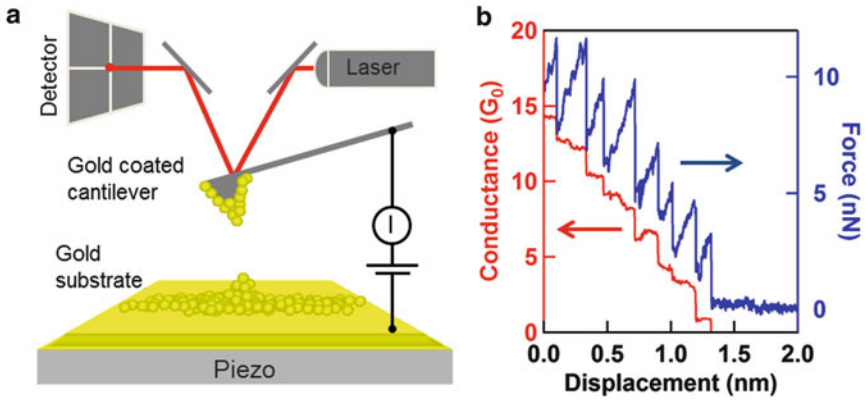

Fig. 12.2 (**a**) Schematic of the modified conductive atomic force microscope. An Au point contact is formed between a Cr/Au-coated cantilever and an Au-coated substrate with the relative separation controlled by a piezo. The force acting on the junction is detected by optically measuring the deflection of the cantilever. (**b**) Sample conductance (*red*) and force (*blue*) data showing the evolution and rupture of an Au point contact, at a bias of 25 mV and a piezo displacement speed of 18 nm/s. Step-wise decreases in conductance are accompanied by sudden jumps in the force

broken, while conductance and force are recorded as a function of sample displacement. This process is repeated thousands of times to obtain large data sets of conductance and simultaneously acquired force versus junction elongation. Before adding any molecule to the substrate, at least 1,000 conductance and force traces were collected to ensure that no contamination was present in the setup. Individual conductance traces for an Au point-contact show stepwise decrease in conductance until a single atom contact is formed with a conductance of $G_0 = 2e^2/h$, the quantum of conductance (Fig. 12.2b). The simultaneously acquired force traces show a characteristic saw-tooth pattern (Fig. 12.2b) indicating two distinct force regimes: gradual linear increases due to elastic (reversible) elongations and sharp drops due to permanent deformations of the junction. Upon further stretching, the single atomic gold wire breaks and the conductance exhibits a tunneling signature when no molecules are present, while the cantilever displacement changes abruptly. When measurements are carried out in an environment of molecules, an additional conductance step is frequently observed at a molecule-dependent conductance value below 1 G_0 along with an additional abrupt change in the force trace. The full trace of force versus elongation presents a rich dataset describing the mechanical evolution of these junctions under stress. In this study, we focus on the force associated with the breaking of a single atomic Au contacts or an Au-molecule-Au junctions. This can be determined by analyzing the change in the cantilever deflection at the location where the 1 G_0 or the molecular conductance step ends and the junction breaks.

To extract statistically significant characteristics from the evolution of junction conductance and force as a function of sample displacement, we construct two-dimensional (2D) histograms from the conductance and force traces, setting the origin of the displacement axis at the point where either the 1 G_0 conductance step or the molecular conductance step breaks. This well-defined position on the x-axis is determined individually for each trace, using an automated algorithm. A fraction of the traces do not show a conductance plateau at G_0 or a plateau corresponding to a molecular junction. It is likely that the absence of the G_0 or the molecular conductance plateau means that a single-atom point contact or a single molecule junction was not formed during that particular measurement. Therefore, these traces were not used for further analysis, as they do not contain the bond rupture event of interest. The statistical occurrence of the junction of interest varies with the case, but a statistically significant and unbiased data set results in each case. Each data point on the digitized conductance (force) trace was thus assigned a conductance (force) coordinate (along the y-axis) and a position coordinate (along the x-axis). Two-dimensional conductance histograms were then generated without further analysis. For the two-dimensional force histogram, we also set the force at the new zero-displacement position to zero force by subtracting an offset from the entire force trace. This realigned all force traces to a common point such that each force and displacement value was now determined relative to the value at the end of the conductance step in each trace. After this realignment, thousands of force traces were added to generate a two-dimensional force histogram. A statistically averaged force profile is obtained from this histogram from the peak of a Gaussian that is fit to vertical sections at every displacement bin.

Figure 12.3a, b shows two-dimensional conductance and force histograms, respectively, constructed from over 31,000 traces measured without any molecules present and using 20 different tip/sample pairs. Insets to Fig. 12.3a, b show a sample conductance and simultaneously acquired force trace, respectively, to illustrate where the zero in displacement is set. The conductance is plotted on a logarithmic axis, whereas the force and the position (x-) axes use linear bins in these plots. Negative displacements are events that occur before the end of the 1 G_0 plateau while positive corresponds to data beyond the

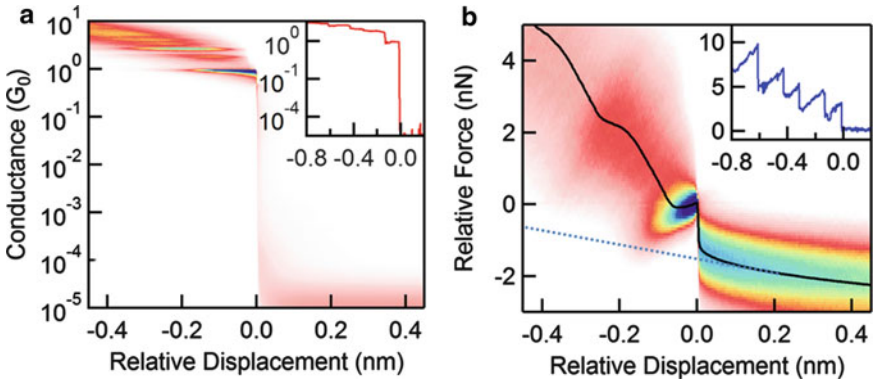

Fig. 12.3 (**a**) Two-dimensional conductance histogram constructed from over 31,000 traces. All traces are aligned such that the end of the plateau at 1 G_0 is at zero along the displacement axis. A large number of counts is visible at integer multiples of G_0. Inset: Sample conductance trace aligned to zero displacement at the end of the 1 G_0 plateau. (**b**) Two-dimensional force histogram constructed from simultaneously acquired force traces. The force profile (*black curve*) is overlaid and shows a clear jump at zero displacement. The rupture force of 1.4 nN for a single atomic contact is determined by extrapolating the fit of the force profile (*dotted line*). Inset: Force trace acquired simultaneously with conductance trace shown in the inset to panel (**a**), aligned at the 1 G_0 break

end of the plateau. These histograms are generated from traces where the G_0 step can be identified with our automated algorithm. Approximately 80% (31,033 out of 39,000) of the measured traces exhibit a clearly identifiable 1 G_0 step and are included. Figure 12.3a shows clear peaks at integer multiples of G_0 occurring at negative displacements, and almost no counts at positive displacements, since zero displacement is set at the point when the G_0 contact breaks.

The 2D force histogram, created from the same set of traces, (Fig. 12.3b) shows a trend in the force that is increasing with increasing displacement, just prior to the clear sharp drop at zero displacement. The force required to break the G_0 contact can be determined from the magnitude of this drop. The force profile is effectively an averaged force trace for the single atom contact rupture event. It shows a clearly defined drop of 1.4 ± 0.2 nN at zero displacement, as illustrated in Fig. 12.3b, corresponding to the breaking force of a single Au-Au bond. This value is in good agreement with published experimental and theoretical results [22–24], validating our 2D analysis method. We note here that this result is from a statistically significant data set of about 31,000 traces, providing a robust and unbiased determination of the single Au-Au bond breaking force.

12.3 Single Molecule Measurements

We apply this same technique to compare the bond rupture force in single molecule junctions. We study seven molecules chosen to represent (a) four different molecular backbones (butane, hexane, benzene and bipyridine), each with a nitrogen termination, and (b) four linker groups (Amine [NH_2], thiomethyl [SMe], thiol [SH] and diphenylphosphine [DPP]), each attached to similar saturated backbones (of 4 or 5 carbon atoms). The chemical names (and abbreviations used in the following discussion) for the molecules are: (a) 1,4 diaminobenzene (BDA), (b) 4,4′ bipyridine (BP), (c) 1,6-hexanediamine (C6A), (d) 1,4-butanediamine (C4A) (e) 1,4-bis(methylsulfide) butane (C4SMe), (f) 1,5 bis-(diphenyl-phosphino)pentane (C5DPP), and (g) 1,4-butanedithiol (C4SH). Each compound is obtained from commercial sources, and used without further purification. Conductance is determined by measuring current through the junction at a constant applied bias of 25 mV for all molecules, except 75 mV for C6A and for BP. The molecules are deposited onto the Au substrate either by evaporation or by addition of a dilute concentration of molecule in the solvent 1,2,4-tricholorobenzene (TCB). Both the conductance and force results are independent of the deposition method. Over 10,000 individual conductance and simultaneously acquired force traces are collected with multiple tip/sample pairs for each molecule and these are analyzed by generating 2D histograms, as detailed above, to characterize the molecular breaking force.

Figure 12.4a shows a 2D conductance histogram for C4A where the origin in the displacement axis is set at the end of the molecular conductance step. Logarithmic bins for the conductance (y-) axis and linear bins for the displacement (x-) axis are chosen for image clarity. The measured traces that show a molecular conductance step were selected using an automated algorithm for both conductance and force analysis. Insets of Fig. 12.4a, b show conductance and simultaneous force data for one particular junction breaking event, out of the over 3,500 individual measurements used to construct the 2D histograms. A clear feature is seen in the conductance histogram at 9×10^{-4} G_0, which gives us the most probable conductance of an

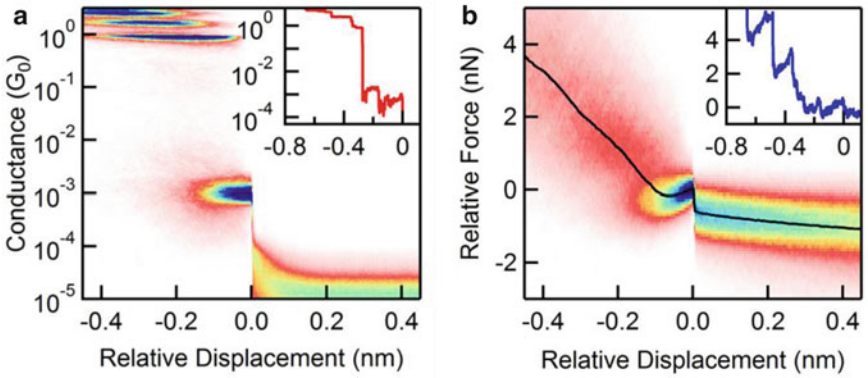

Fig. 12.4 (**a**) Two-dimensional conductance histogram of C4A constructed from over 3,500 traces with a molecular conductance step. Features representing a sequence of Au contacts clearly appear at integer multiples of G_0. A molecular signature can be clearly seen at 9×10^{-4} G_0. Inset: A sample conductance trace showing a G_0 and molecular plateau with zero displacement set to the end of the molecular plateau. (**b**) The two-dimensional force histogram for C4A is constructed from the simultaneously acquired force traces of the same set of traces used to construct the conductance histogram. The average force profile (*black curve*) shows a clear drop at zero-displacement, which gives a statistically determined breaking force for the N-Au bond of ~0.6 nN. Inset: The simultaneously acquired force trace aligned after the molecular step is shown

Au-C4A-Au junction. This peak extends over a displacement of about 0.15 nm, indicating that molecular junctions can be elongated over this distance prior to the final rupture.

Every molecule, except C4SH, shows characteristic conductance features due to the selective binding of the N, SMe or DPP linker to undercoordinated Au atoms [26, 27]. Particularly, BP shows two characteristic conductance peaks (a 'high-G' and a 'low-G' peak) that occur at distinct junction elongation distances [28–30]. In this work, we probe the rupture from the low-G peak, which corresponds to a geometry where the molecule bridges the two Au electrodes vertically [30]. Except C4SH, for which we do not find any well-defined conductance, we note that the conductance peak positions (corresponding to the most frequently measured conductance, see Table 12.1) are in good agreement with previously published data collected in solution using the scanning tunneling microscope-based break junction technique [27, 30]. This further validates our measurement and molecule deposition techniques. Furthermore, the clear conductance signature seen for all these molecules allows us to measure specific single Au-molecule-Au junction rupture events unambiguously. In each case, except the thiolate (SH) linker, it is also known that the binding mechanism is the (N, P or S)-Au donor-acceptor interaction [26, 27, 30–33]. In Table 12.1, we show bond rupture forces determined from 2D force histograms for six molecules considered here, except C4SH. We see that in all these cases, the Au-molecule-Au junction ruptures at a force smaller than that of an Au-Au bond, indicating that rupture occurs at the respective donor-acceptor bonds consistent with earlier work [16, 27, 33]. Specifically in the amine linked molecules, by comparing the measured rupture forces for C4A and C6A we see first that for these two alkanes with 4 and 6 carbons in the backbone, the rupture forces are very similar. Additionally, we see that the force required to break the N-Au bond in the conjugated molecule, BDA, is considerably smaller than in C4A and C6A, which are fully saturated.

For the thiol (SH) linker, there are multiple bonding scenarios for an Au-S covalent bond, many possible locations for the adsorption of the H atom on the electrodes and also a possibility of forming an Au-SH donor-acceptor bond [34]. In our conductance results of C4SH, we see a qualitatively different behavior from those of the other three linkers. We see a multitude of conductance features over a wide range of conductance spanning from just below G_0 to the experimental noise floor. This fact reflects previous studies [35, 36] which have explained such observations based on the many possible binding mechanisms and geometries accessible to thiol linkers. Figure 12.5a, c demonstrates the lack of any clear conductance feature in individual measurements of C4SH, in comparison to measurements with C4SMe, in our experiments. This precludes the unambiguous assignment of the displacement at which the junction ruptured in each trace, which is essential in constructing a 2D conductance or force histogram. We therefore focus the analysis on the force traces, and use an alternate approach, based on identification of all sharp drops in individual force traces with an automated algorithm. Each force drop corresponds either to a structural rearrangement in the junction or junction rupture. Each such event can be associated with the conductance of the junction immediately prior to the abrupt jump in force. One key difference between the 2D force analysis technique used above and this alternate force event identification method is that the former relies on the identification of events through conductance and therefore does not bias the results towards larger force values that are more easily identified.

Table 12.1 Comparison of most frequently measured conductance and rupture force for molecular junctions with a nitrogen termination having different backbones (rows 1–4) and saturated backbones having different linker groups (rows 4–6)

No.	Molecule	Chemical structure	Conductance (G_0)	Bond rupture force (nN)	
				Expt.	DFT
1	1,4 benzenediamine (BDA)	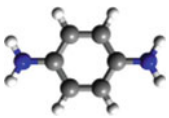	6×10^{-3}	0.5	0.46
2	4,4′ bipyridine (BP)	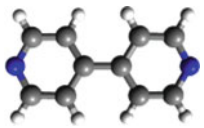	1×10^{-4}	0.8	1.00
3	1,6 hexanediamine (C6A)	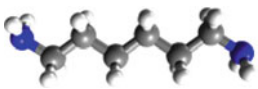	1×10^{-4}	0.6	–
4	1,4 butanediamine (C4A)	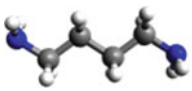	9×10^{-4}	0.6	0.84
5	1,4-bis(methylsulfide) butane (C4SMe)	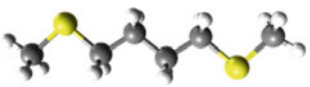	1×10^{-3}	0.7	0.84
6	1,5 bis-(diphenyl-phosphino)-pentane (C5DPP)	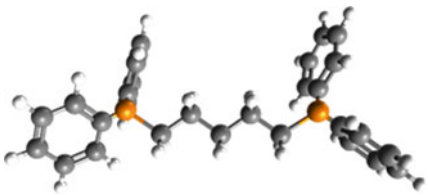	7×10^{-4}	0.8[a]	1.4[b]

Rupture forces predicted by DFT adiabatic trajectory simulations of representative junctions are also listed for quantitative comparison
[a]Experiments with C5DPP showed evidence of significant fluctuations in force over the course of individual molecular conductance signatures
[b]DFT calculations for butane with dimethylphosphine links [33]

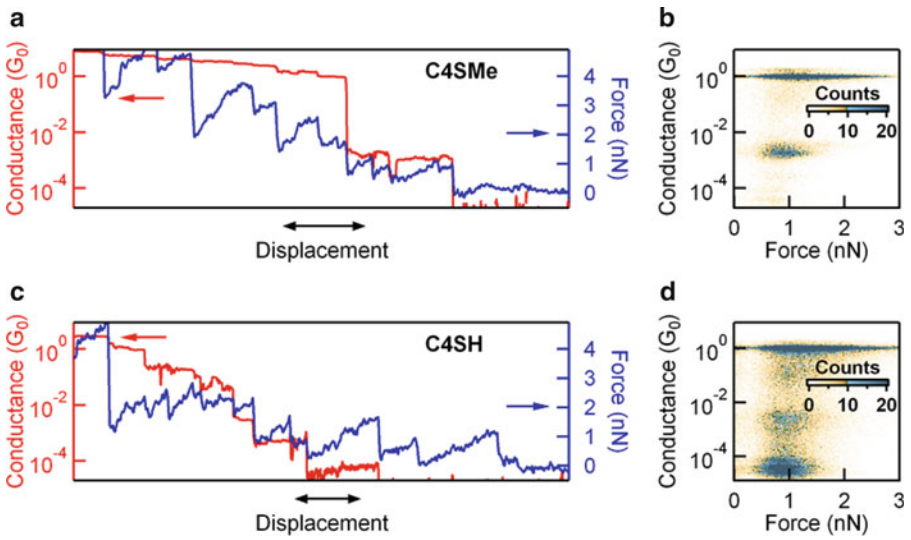

Fig. 12.5 Sample conductance (*red*) and force (*blue*) traces for C4SMe (**a**) and C4SH (**c**). The *double headed arrows* indicate a 0.2 nm displacement. 2D histograms showing each identified force drop event and its corresponding conductance value for C4SMe (**b** – 51,000 events) and C4SH (**d** – 121,000 events). The conductance bin size is 30 bins per decade, and the force bin size is 0.04 nN

In Fig. 12.5b, d we show the two-dimensional histograms correlating the change in force for each force event against the associated conductance immediately prior to the force event from all measured traces for C4SMe and C4SH. Each count in this 2D histogram represents a force and conductance value of an individual trace, as determined by the automated algorithm. We see first that both histograms show a large number of force events at a conductance value around 1 G_0. These force events correspond to rearrangement and the final breaking of a single-atom gold contact. Second, for C4SH (Fig. 12.5d), we find numerous force events spread along the conductance axis from just below 1 G_0 to the experimental conductance noise floor of about 2×10^{-5} G_0. For C4SH, we find that 75% of all measured traces exhibit force events with a conductance below 1 G_0. Furthermore, from this selected subset, we find that each trace has an average of 2.7 force events. This is a direct indication that junctions formed with the S-Au bond undergo substantial rearrangements with varied atomic structure that sustain a broad range of conductance values. In contrast, the C4SMe data (Fig. 12.5b) shows that almost all force events below 1 G_0 occur within a narrowly defined conductance range [33]. Of all the measured traces, 40% show force events for a conductance below 1 G_0, and of this subset, each trace has an average of 1.5 force events. Thus although some structural rearrangement might occur in SMe terminated molecular junctions, they are not accompanied by large changes in conductance. This agrees with previous DFT based junction elongation simulations that show shifts in attachment point for the donor-acceptor bond with modest changes in junction conductance [33]. Finally, the C4SH data also shows a significant number of force events with conductance values within our experimental noise; a large number of force events occur at a conductance that is too low to measure in this set-up. This could be due to the formation of molecular dimers or due to pulling out of chains of gold atoms, as has been seen in simulations [37–40].

12.4 Discussion

We have used DFT-based calculations to simulate the junction elongation [40, 41] process and to understand the trends in the rupture forces for the molecules studied here. Representative junction structures are developed with similar orientation and link bonding for comparisons. Each Au tip and surface were modeled with an Au pyramid (20 atoms each) with (111) surfaces with the tip atom on the top pyramid moved to an adatom site on one facet resulting in a blunt, three atom tip [33]. Here we focused on the portion of the trajectory where the junction was elongated from a local energy minimum through the inflection point and finally probed the dissociated structure after one bond ruptures. The back layer of Au atoms in each pyramid was held fixed with a bulk lattice parameter of 4.08 Å. All other degrees of freedom were relaxed until all forces were less than 0.005–0.01 eV/Å for each junction structure. The junction was elongated in steps of 0.05–0.1 Å by increasing the separation between the pyramids along the z direction and then fully optimizing the geometry. Density functional theory total energy calculations and geometry optimization were performed with the VASP package [42], using the projector augmented wave approach which naturally included scalar relativistic effects for Au [43, 44] and the generalized gradient approximation (GGA) of Perdew, Burke, and Ernzerhof (PBE) [45] for the exchange-correlation density functional. The model junction was placed in a hexagonal supercell ($a = 2.0$ nm, $c = 3.5$ nm) and the basis set for solution of the Kohn-Sham equations was determined by a 400 eV cutoff.

The qualitative features of the calculated energy and force curves of an adiabatic junction trajectory are demonstrated in Fig. 12.6a. In this case the calculations were performed by pulling on a C4SMe junction (Fig. 12.6b). Under the application of increasing force due to junction elongation, the total energy increases from its local minimum value. Finally, a maximum sustained force value (here ~0.8 nN) is reached. In these junction structures, the link bonds are not identical. One of the two undergoes most of the elongation and after the maximum sustained force that link bond length rapidly increases, corresponding to bond rupture. The calculated values listed for the maximum sustained force in Table 12.1 represent model structures for each junction with similar backbone orientation, giving a good basis for assessing chemical trends. They do generally represent a single adiabatic junction elongation trajectory. However, our previous studies [33] have shown that small changes in junction structure (attachment point or molecule orientation) can lead to ~0.1–0.2 nN variations in the maximum sustained force. More generally, we can also expect that diverse junction structures are sampled in the experiments, including variations in Au-linker bond orientation in the junction and relative to the pulling direction (Fig. 12.6c–f).

With due considerations for the variations in junction structures as well as the fluctuations due to temperature and mechanical vibrations encountered in experiments, there is a good agreement between the DFT calculations of maximum sustained force and experimental rupture forces. For the phosphine links (C5DPP in the experiments), calculations suggested a substantially larger maximum sustained force. The typical maximum sustained force for the Au-P donor-acceptor bond was around 1.4 nN for butane with the dimethylphosphine linker and there were clear indications that the stress is sufficient to rearrange the local Au atomic arrangement near the link bond [27, 33]. However, the selectivity of the link bonding motif,

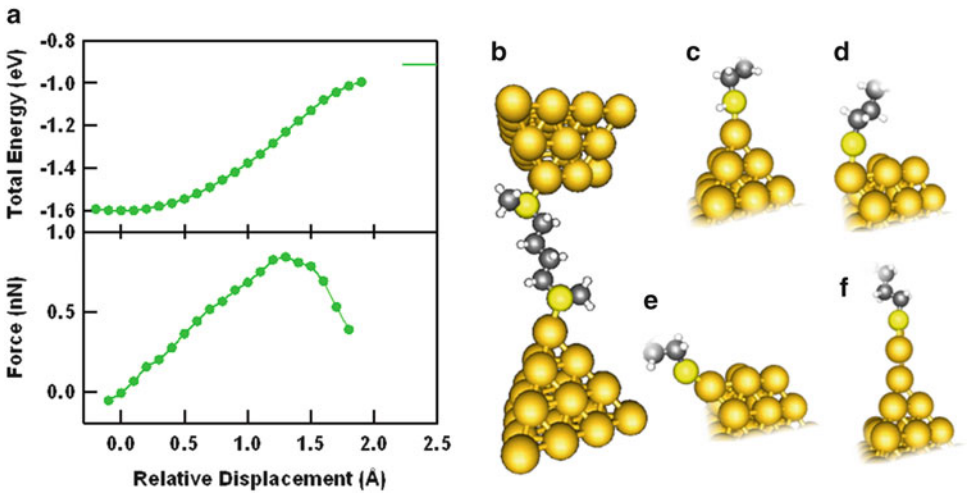

Fig. 12.6 (**a**) Calculated total energy (*top*) and force (*bottom*) curves from an adiabatic trajectory calculation for C4SMe, shown as a function of displacement. Bar shown at right indicates the asymptotic value. This calculation demonstrates the typical qualitative features of single-molecule junctions with donor-acceptor interactions. (**b**) Snapshot of the C4SMe junction structure near the local energy minimum. (**c**–**f**) Illustrations of possible contact structures in single-molecule junctions formed with C4SH. Scenarios include: (**c**) H atom remains on the S, (**d**) Au atom is not at the apex of the electrode, (**e**) junction is formed at an angle, and (**f**) Au atom coordination is altered due to chain formation

to specific undercoordinated Au atomic sites, still results in the well-defined conductance plateaus. In phosphine linked junctions, modest steps in conductance are often observed in individual experimental traces that may correspond to rearrangement. Qualitatively, the DFT-based simulations are consistent with the measurements, but the relatively low measured average rupture force has not been explained. One possibility is that constraints in full junction formation (bonds to substrate and tip, accommodating the bulky tertiary phenyl groups) result in structures where the donor-acceptor bonds are weaker than optimal. The rearrangement of the local Au atomic structure may also be significant.

For junctions with S-Au linkage, DFT based calculations have indicated that selected scenarios support a maximum sustained Au-S bond force in excess of 1.5 nN [41, 46]. More strikingly, detailed molecular dynamics simulations of thiol linked junction evolution show a rich series of rupture/rearrangement events with the molecule removing one or more Au atoms in the final, ruptured state [37–40]. Also, the position and resulting effects of the hydrogen from the SH can lead to drastic changes in force and conductance values [40, 41, 46, 47]. The experimental behavior of conductance and force trajectories for C4SH junctions, summarized in Fig. 12.5c, d, are consistent with a sustained force that is sufficient to drive substantial rearrangement of the local structure during elongation. However, most of these events occur with a change in force that is substantially less than the average force required to rupture the Au point contact. This does not imply that they do not break at the Au-Au bond. Molecular dynamics simulations illustrate that junctions formed with Au-S links can result in contact structures that have varied geometries. In contrast to the idealized structure (Fig. 12.6c), the terminal Au atom could be on the side of an electrode structure (Fig. 12.6d), the constraints on junction formation with two distinct link bonds, one to each electrode, can result in an angle between the backbone and the pulling direction (Fig. 12.6e), and the coordination of the Au atom to which the S is bonded can be altered (Fig. 12.6f). A key factor is the strength of the Au-S bond relative to the softness of the Au resulting in local rearrangement under stress [37–40]. Our calculated adiabatic trajectories for selected scenarios illustrate that the maximum sustained force can be both larger and smaller than the nominal Au single point contact rupture force, depending on the structure. A broader-based survey of structure as well as investigation of the role of thermal fluctuations and solvent interactions will be essential to fully understand the measured rupture forces in cases like thiol bonded junctions with strong bonds to Au. The occurrence of these non-ideal evolution scenarios is supported by our experimental results for conductance and force of C5DPP and C4SH single molecule junctions.

In summary, we demonstrated an experimental approach to simultaneously measure force and conductance data for single molecular junctions, developing and establishing a new, two-dimensional histogram method to statistically evaluate thousands of individual measurements. This method leads to an experimentally determined average breaking force of a single Au-Au bond of 1.4 nN, based on over 31,000 individual measurements. Using a set of N terminated molecules, we showed that the electronic structure of the molecular backbone alters N-Au bond strengths considerably, as can be seen both in the calculations and measurements: 1,4-benzenediamine binds most weakly to Au atoms, while the pyridine-gold bond exhibits the largest breaking force among the molecules considered here. We then presented measurements for four different chemical linker groups connected to saturated backbones. Analyzing this data using the 2D conductance and force

histograms, we have shown that amine, methylsulfide, and diphenylphosphine linkers break in a molecular junction with a most probable breaking force of about 0.6, 0.7, and 0.8 nN respectively, indicating rupture at the donor-acceptor linkage. In the case of thiol linkers, we compiled force and conductance data from individual traces, since we did not observe a well-defined molecular conductance signature. Correlating the occurrence of force events with conductance, we find that C4SH junctions on average have more force events per trace than C4SMe. This observation supports the notion that a strong covalent sulfur-gold bond drives more significant rearrangement of these molecular junctions. By combining simultaneous measurement of force and conductance with statistical analysis and DFT simulations we obtain a quantitative insight into the electronics and mechanics of single-molecule junctions. In the future, these results can help us understand and engineer molecular electronic devices with varied functionality.

Acknowledgements This work was supported by the National Science Foundation (Career Award CHE-07-44185) and by the Packard Foundation. A portion of this work was performed using facilities in the Center for Functional Nanomaterials at Brookhaven National Laboratory and supported by the U.S. Department of Energy, Office of Basic Energy Sciences, under Contract No. DE-AC02-98CH10886.

References

1. Aviram A, Ratner MA (1974) Molecular rectifiers. Chem Phys Lett 29(2):277–283
2. Gimzewski JK, Joachim C (1999) Nanoscale science of single molecules using local probes. Science 283(5408):1683–1688
3. Joachim C, Gimzewski JK, Aviram A (2000) Electronics using hybrid-molecular and mono-molecular devices. Nature 408(6812):541–548
4. Nitzan A, Ratner MA (2003) Electron transport in molecular wire junctions. Science 300(5624):1384–1389
5. Reed MA et al (1997) Conductance of a molecular junction. Science 278(5336):252–254
6. Smit RHM et al (2002) Measurement of the conductance of a hydrogen molecule. Nature 419(6910):906–909
7. Reichert J et al (2002) Driving current through single organic molecules. Phys Rev Lett 88(17):176804
8. Xu B, Tao NJ (2003) Measurement of single-molecule resistance by repeated formation of molecular junctions. Science 301(5637):1221–1223
9. Venkataraman L et al (2006) Dependence of single-molecule junction conductance on molecular conformation. Nature 442(7105):904–907
10. Reddy P et al (2007) Thermoelectricity in molecular junctions. Science 315(5818):1568–1571
11. Widawsky JR et al (2012) Simultaneous determination of conductance and thermopower of single molecule junctions. Nano Lett 12 (1):354–358
12. Li C et al (2007) Charge transport in single Au/alkanedithiol/Au junctions: coordination geometries and conformational degrees of freedom. J Am Chem Soc 130(1):318–326
13. Martin S et al (2010) The impact of E-Z photo-isomerization on single molecular conductance. Nano Lett 10(6):2019–2023
14. Taniguchi M et al (2011) Dependence of single-molecule conductance on molecule junction symmetry. J Am Chem Soc 133(30):11426–11429
15. Grandbois M et al (1999) How strong is a covalent bond? Science 283(5408):1727–1730
16. Xu BQ, Xiao XY, Tao NJ (2003) Measurements of single-molecule electromechanical properties. J Am Chem Soc 125(52):16164–16165
17. Frei M et al (2011) Mechanics and chemistry: single molecule bond rupture forces correlate with molecular backbone structure. Nano Lett 11 (4):1518–1523
18. Frei M et al (2012) Linker dependent bond rupture force measurements in single-molecule junctions. J Am Chem Soc 134(9):4003–4006
19. Aradhya SV et al (2012) Dissecting contact mechanics from quantum interference in single-molecule junctions of stilbene derivatives. Nano Lett 12(3):1643–1647
20. Dudko O, Hummer G, Szabo A (2006) Intrinsic rates and activation free energies from single-molecule pulling experiments. Phys Rev Lett 96 (10):108101
21. Evans E (2001) Probing the relation between force–lifetime–and chemistry in single molecular bonds. Annu Rev Biophys Biomol Struct 30:105–128
22. Rubio-Bollinger G et al (2001) Mechanical properties and formation mechanisms of a wire of single gold atoms. Phys Rev Lett 87(2):026101
23. Rubio G, Agraït N, Vieira S (1996) Atomic-sized metallic contacts: mechanical properties and electronic transport. Phys Rev Lett 76 (13):2302–2305
24. Tavazza F, Levine LE, Chaka AM (2009) Elongation and breaking mechanisms of gold nanowires under a wide range of tensile conditions. J Appl Phys 106(4):043522
25. Hutter JL, Bechhoefer J (1993) Calibration of atomic-force microscope tips. Rev Sci Instrum 64(7):1868–1873
26. Venkataraman L et al (2006) Single-molecule circuits with well-defined molecular conductance. Nano Lett 6(3):458–462
27. Park YS et al (2007) Contact chemistry and single-molecule conductance: a comparison of phosphines, methyl sulfides, and amines. J Am Chem Soc 129(51):15768–15769
28. Tam ES et al (2011) Single-molecule conductance of pyridine-terminated dithienylethene switch molecules. ACS Nano 5(6):5115–5123
29. Kamenetska M et al (2010) Conductance and geometry of pyridine-linked single-molecule junctions. J Am Chem Soc 132(19):6817–6821
30. Quek SY et al (2009) Mechanically controlled binary conductance switching of a single-molecule junction. Nat Nanotechnol 4(4):230–234
31. Hybertsen MS et al (2008) Amine-linked single-molecule circuits: systematic trends across molecular families. J Phys Condens Mater 20 (37):374115
32. Parameswaran R et al (2010) Reliable formation of single molecule junctions with air-stable diphenylphosphine linkers. J Phys Chem Lett 1 (14):2114–2119
33. Kamenetska M et al (2009) Formation and evolution of single-molecule junctions. Phys Rev Lett 102(12):126803

34. Basch H, Cohen R, Ratner MA (2005) Interface geometry and molecular junction conductance: geometric fluctuation and stochastic switching. Nano Lett 5(9):1668–1675
35. Ulrich J et al (2006) Variability of conductance in molecular junctions. J Phys Chem B 110(6):2462–2466
36. Arroyo CR et al (2011) Influence of binding groups on molecular junction formation. J Am Chem Soc 133(36):14313–14319
37. Strange M, Lopez-Acevedo O, Hakkinen H (2010) Oligomeric gold-thiolate units define the properties of the molecular junction between gold and benzene dithiols. J Phys Chem Lett 1(10):1528–1532
38. Krüger D et al (2002) Pulling monatomic gold wires with single molecules: an ab initio simulation. Phys Rev Lett 89(18):186402
39. Li Z, Kosov DS (2007) Nature of well-defined conductance of amine-anchored molecular junctions: density functional calculations. Phys Rev B 76(3):035415
40. Paulsson M et al (2009) Conductance of alkanedithiol single-molecule junctions: a molecular dynamics study. Nano Lett 9(1):117–121
41. Qi YH et al (2009) Breaking mechanism of single molecular junctions formed by octanedithiol molecules and Au electrodes. J Am Chem Soc 131(45):16418–16422
42. Kresse G, Furthmuller J (1996) Efficient iterative schemes for ab initio total-energy calculations using a plane-wave basis set. Phys Rev B 54 (16):11169–11186
43. Kresse G, Joubert D (1999) From ultrasoft pseudopotentials to the projector augmented-wave method. Phys Rev B 59(3):1758–1775
44. Blochl PE (1994) Projector augmented-wave method. Phys Rev B 50(24):17953–17979
45. Perdew JP, Burke K, Ernzerhof M (1996) Generalized gradient approximation made simple. Phys Rev Lett 77(18):3865–3868
46. Li ZL, Zhang GP, Wang CK (2011) First-principles study on formation and electron-transport properties of single oligothiophene molecular junctions. J Phys Chem C 115(31):15586–15591
47. Cossaro A et al (2008) X-ray diffraction and computation yield the structure of alkanethiols on gold(111). Science 321(5891):943–946